Relation between Denaturation Time Measured by Optical Coherence Reflectometry and Thermal Lesion Depth during Radiofrequency Cardiac Ablation: Feasibility Numerical Study

Ana González-Suárez[1*], David Herranz[2], Enrique Berjano[3], Jose L Rubio-Guivernau[2], Eduardo Margallo-Balbás[2]

[1] Department of Information and Communication Technologies, Universitat Pompeu Fabra, Barcelona, Spain, [2] Medlumics S.L, Tres Cantos, Spain, [3] BioMIT, Department of Electronic Engineering, Universitat Politècnica de València, Valencia, Spain

*Correspondence to: Ana González-Suárez, PhD, Department of Information and Communication Technologies, Universitat Pompeu Fabra, Carrer Roc Boronat 138, 08018 Barcelona, Spain; Email: ana.gonzalez@upf.edu

Conflict of interest Disclosures: All authors have completed and submitted the ICMJE Form for Disclosure of Potential Conflicts of Interest and none were reported

Abstract

Background/Objective: Radiofrequency (RF) catheter ablation is a minimally invasive medical procedure used to thermally destroy the focus of cardiac arrhythmias. Novel optical techniques are now being integrated into RF catheters in order to detect the changes in tissue properties. Loss of birefringence due to fiber denaturation at around 70ºC is related to changes in accumulated phase retardation and can be measured by polarization-sensitive optical coherence reflectometry (PS-OCR). Since irreversible thermal lesions are produced when the tissue reaches 50ºC, our goal was to seek the mathematical relationship between both isotherms.

Materials and Methods: A two-dimensional model based on a coupled electric-thermal problem was built and solved using the finite element method. The model consisted of cardiac tissue, blood and a non-irrigated electrode with a sensor embedded in its tip to maintain a specific target electrode temperature. Computer simulations were conducted by varying the tissue characteristics. Lesion depth was estimated by the 50ºC isotherm, while the denaturation time (TD) was taken as the time at which the 70ºC isotherm reached a depth of 0.75 mm (which corresponds to the optical depth reached by PS-OCR technology).

Results: A strong correlation (R^2>0.83) was found between TD and lesion depth and an even stronger correlation (R^2>0.96) was found between TD and the time required to achieve a specific lesion depth. For instance, the ablation time required to ensure a minimum lesion depth of 3 mm was $1.33 \times TD + 3.93$.

Conclusions: The computer results confirmed the strong relationship between denaturation time and lesion depth and suggest that measuring denaturation time by PS-OCR could

provide information on the ablation time required to reach a specific lesion depth.

Keywords: Cardiac ablation, computer model, polarization-sensitive optical coherence reflectometry, radiofrequency ablation.

INTRODUCTION

The clinical success of radiofrequency ablation (RFA) for atrial fibrillation depends on achieving a transmural lesion, i.e. a lesion that occupies the entire thickness of the atrial wall [1]. Since this can be as little as 2 mm [2], and may be close to the esophagus [3,4], it is thus crucial to ensure a specific lesion depth. Different technologies have attempted to evaluate lesion size [5-8], but the correlation of their parameters with lesion size was seen to be low. Optical techniques such as optical coherence reflectometry (OCR) or polarimetry seem to be the most appropriate technology due to their high resolution in the thin wall [9]. Recently, optical polarimetry [10] has been successfully used to detect lesion size in excised myocardial sections, although depth-resolved birefringence measures are required to study the evolution of the lesion over time in clinical conditions. OCR is a non-invasive high-resolution imaging technique capable of sampling the internal optical properties of biological tissues by measuring the intensity of back reflected light as a function of depth. The authors considered that this technique could improve RF cardiac ablation of atrial fibrillation. Polarization sensitive OCR (PS-OCR) is a functional extension of OCR that measures depth-resolved birefringence [11], an optical property of an anisotropic medium, by which the propagation velocity of the light traveling through the medium depends on the polarization state of the light. Muscular tissue is known to exhibit birefringent properties [12,13], but loses its

anisotropic ultrastructure due to protein denaturation when exposed to temperatures of around 70ºC [14]. A new integrated catheter was therefore designed to enable simultaneous RFA and PS-OCR operation [15,16]. This catheter is able to measure denaturation time (TD), which is the time at which the optical birefringence of the tissue 0.75 mm below the surface (PS-OCR spatial window) is completely lost. While TD is related to the progress of the 70ºC isotherm [14], the thermal lesion is known to be related to the 50ºC isotherm [17].

OBJECTIVES

The objective of the present work was thus to model the relationship between the lesion depth (assessed by the 50ºC isotherm) and denaturation time (TD), which is the time at which the 70ºC isotherm reaches a depth of 0.75 mm (equivalent to the denaturation contours of fibers in an experimental scenario). The mathematical relationship obtained between TD and lesion depth would allow algorithms to be implemented to enable real-time monitoring of lesion depth by PS-OCR images.

MATERIALS AND METHODS

As computational models are a powerful, fast and cheap tool to attain useful information on the electrical-thermal processes associated with energy-based therapies [18-21], this method was used to simulate the electric, thermal and tissue damage response of a two-dimensional model of cardiac tissue subjected to RF ablation.

Model geometry

Figure 1 shows the model geometry, including a fragment of cardiac tissue, a volume of blood (cardiac chamber), and a non-irrigated electrode (7Fr diameter and 4 mm long). Although irrigated electrodes are usually employed to ablate atrial tissue, we first focused on a non-irrigated electrode as it provides a very simple temperature distribution in which the hottest point is at the electrode–tissue interface. The catheter was assumed to be perpendicular with respect to the cardiac tissue and inserted to a depth of 0.5 mm (no realistic details were required on the mechanical deformation of the tissue surface due to the electrode, since this value was assumed to be lower than 2 mm [22]). The electrode included a sensor embedded in its tip (thermistor 0.75 × 0.3 mm), which was used to monitor the electrode temperature [23]. The dispersive electrode was modeled as an electrical boundary condition at a distance from the active electrode, while the voltage applied to the active electrode was modulated throughout the ablation in order to keep the electrode temperature approximately constant at T_{target}.

Cardiac tissue thickness (H) was 20 mm [23] and the dimensions of the cardiac chamber (X and Z) were estimated by means of a convergence test in order to avoid boundary effects. In this test, the value of the maximal temperature achieved in the tissue (T_{max}) after 60 s of RF heating was used as control parameter. We first considered a tentative spatial (i.e. minimum meshing size) and temporal resolution. To determine the appropriate parameters of X and Z, we increased their values by equal amounts. When the difference in the T_{max} between consecutive simulations was less than 0.5%, we considered the former values to be adequate. We then determined adequate spatial and temporal resolution by means of similar

convergence tests using the same control parameter as in the previous test. Discretization was spatially heterogeneous: the finest zone was always the electrode-tissue interface, where the largest voltage gradient was produced and hence the maximum value of current density. In the tissue, grid size was increased gradually with distance from the electrode-tissue interface.

Governing equations

The model was based on a coupled electric-thermal problem, which was solved numerically using the Finite Element Method (FEM) with COMSOL Multiphysics software (COMSOL, Burlington, MA, USA). The governing equation for the thermal problem was the *Bioheat Equation*, modified by the enthalpy method [24,25], which includes the phase change to model tissue vaporization:

$$\frac{\partial(\rho h)}{\partial t} = \nabla \cdot (k \nabla T) + q - Q_p + Q_m \qquad (1)$$

where ρ was density (kg/m^3), h enthalpy, t time (s), k thermal conductivity (W/m·K), T temperature (ºC), q the heat source caused by RF power (W/m^3), Q_p the heat loss caused by blood perfusion (W/m^3) and Q_m the metabolic heat generation (W/m^3). Q_p was not considered since its effect is expected to be minor [26]. Likewise, Q_m was not considered because its effect is negligible in comparison to the other terms [27]. In biological tissues, enthalpy is related to temperature by the following expression [24,25]:

$$\frac{\partial(\rho h)}{\partial t} = \frac{\partial T}{\partial t} \cdot \begin{cases} \rho_l c_l & 0 \le T \le 99^{o}C \\ H_{fg} C & 99 < T \le 100^{o}C \\ \rho_g c_g & T > 100^{o}C \end{cases} \qquad (2)$$

where ρ_i and c_i were the density and specific heat of cardiac tissue before phase-change (i.e. liquid phase, $i=l$) and post-phase-change (i.e. gas phase, $i=g$), respectively; H_{fg} was the latent heat and C the tissue water content. We considered a latent heat value of 2.162×10^9 J/m^3 which corresponds to the product of the water vaporization latent heat (2257 kJ/kg), the water density at 100ºC (958 kg/m^3), and the tissue water content inside the cardiac tissue (75%).

At the frequencies used in RF heating and over the distance of interest, the biological medium can be considered almost totally resistive, and a quasi-static approach can therefore be used to solve the electrical problem [28]. The distributed heat source q is then given by $q = \sigma|\boldsymbol{E}|^2$, where $|\boldsymbol{E}|$ is the magnitude of the vector electric field (V/m) and σ the electrical conductivity (S m^{-1}). $\boldsymbol{E} = -\nabla\Phi$ is calculated from the gradient of the voltage Φ (V), which, in absence of internal electric sources, satisfies $\nabla\cdot(\sigma\nabla\Phi) = 0$.

The Arrhenius (Ω) function was also employed to estimate the relation between the concentrations of native fibers at the initial time *C(0)*, and no denatured fibers at instant τ, *C(τ)*, estimating the percentage of irreversibly damaged tissue [29]:

$$\Omega = \ln\left\{\frac{C(0)}{C(\tau)}\right\} = \int_0^{\tau} A e^{\frac{-E_a}{RT(t)}} dt \qquad (3)$$

where τ was the heating time (s), R the gas constant (8.314 J/K mol), A the frequency factor (s^{-1}), and E_a the activation energy for the irreversible damage (J/mol). The parameters A and E_a depend on the tissue, and specifically for cardiac tissue was considered $A = 2.94\times10^{39}$ s^{-1} and $E_a = 2.596\times10^5$ J/mol [30].

Model parameters

Table 1 shows the thermal and electrical properties of the model elements (electrode, thermistor, catheter, cardiac chamber and cardiac tissue) [23]. The cardiac tissue characteristics were varied in a range according to the literature [31,32] (see Table 2). The initial model temperature was 37ºC. The electrical (σ) and thermal (k) conductivities of cardiac tissue were temperature-dependent piecewise functions: for σ we considered an exponential growth of +1.5%/ºC up to 100ºC [33], where σ_o was the value of the electrical conductivity assessed at 37ºC (see Table 2), which was then reduced by 4 orders for five degrees to model the tissue desiccation process [35], after which it remained constant. k grew linearly 0.12%/ºC up to 100ºC, k_o being the value of the thermal conductivity assessed at 37ºC (see Table 2), after which k was kept constant [35]. Other model parameters, T_{target} and thermal convective coefficients between blood and tissue/electrode (h_T and h_E), were chosen in a range which is believed to be representative of relevant ablation conditions. The effect of changing the value of thermal convective coefficients at the electrode-blood and tissue-blood interface simulates different blood velocities according to the position of the ablating electrode in the cardiac chamber [36].

Boundary conditions

Figure 2a shows the electrical boundary conditions. We considered a constant temperature ablation protocol, which is the usual ablation mode for non-irrigated electrodes in RFA. We implemented a proportional-integral (PI) control algorithm [23,37] using MATLAB (MathWorks, Natick, MA, USA) and the applied voltage was modulated to maintain the temperature in the sensor at T_{target}. A Dirichlet voltage boundary condition was

therefore applied to the active electrode surface. All the outer surfaces of the model except the bottom surface were fixed to zero electric flux (Neumann boundary condition). The voltage on the bottom surface was set to 0 V (dispersive electrode) to mimic a monopolar configuration in which RF current was forced to flow between the active and dispersive electrodes.

Regarding the thermal boundary conditions (Figure 2b), a null thermal flux was used on the symmetry axis and a constant temperature of 37ºC was fixed on the outer surfaces of the model at a distance from the ablating electrode (this was also the initial temperature value). The effect of blood circulating inside the cardiac chamber was modeled by thermal convection coefficients at the electrode–blood (h_E) and the tissue–blood (h_T) interfaces, considering electrical conductivity of blood independent of temperature (as in Method 2 in [23]). We calculated the control coefficients (see Table 2) according to Method 2 explained in [23] considering a blood velocity value of 0.01 m/s.

Analyzed parameters

The thermal lesion depth was assessed using the 50ºC isotherm, which is usually considered to reasonably represent the isotherm of irreversible myocardial injury in hyperthermic ablation [23]. The 70ºC isotherm was also computed since is strongly related with the birefringence change in fibers, and hence with changes in the optical signal of phase retardation (PR) [14]. Figure 3 shows the expected progress of the depths of the 50ºC and 70ºC isotherms (ISO-50ºC and ISO-70ºC, respectively). In the context of this study we were also interested in identifying the following specific instants: 1) the time when the 70ºC isotherm reaches a depth of 0.75 mm (denaturation time (TD)) as this value is approximately

the depth at which the background noise is clearly negligible for PS-OCR images in the integrated catheter [15]; and 2) the times when the 50ºC isotherm reaches a depth of 2, 3 and 4 mm (t_{2mm}, t_{3mm} and t_{4mm}), as these values are relevant in the context of RFA in the atrial wall.

RESULTS

Temperature distributions and thermal damage

Figure 4(a) shows the computed temperature distributions around the ablation electrode. The contour where optical birefringence is expected to be lost due to fiber denaturation (i.e. 70ºC isotherm, ISO-70ºC) correlated well with the $\Omega = 4.6$ isoline (calculated from Equation 3), and extended above the area of thermal lesion assessed with the 50ºC isotherm (ISO-50ºC). Figure 4(b) shows the time course of the percentage of denatured fibers across the depth of the tissue. It is interesting to note that at ~12 s there is a zone of tissue at a depth of ~0.75 mm where the fibers have been almost 100% denatured.

Relationship between denaturation time and thermal lesion depth

Figure 5 shows the strong correlation ($R^2>0.96$, $p < 0.05$) found between the depth of the 50ºC (D50) and 70ºC (D70) isotherms for different ablation times. This finding is certainly the first step in exploring how measuring the denaturation time (TD) could be used to predict lesion depth. In this respect, Figure 6 shows the relationship between the TD (in seconds), assessed as the time at which the 70ºC isotherm reaches 0.75 mm, and the

thermal lesion depth at that time (D_{TD}, in mm). The following linear relationship was found:

$$D_{TD} = 0.035 \times TD + 2.33 \quad (4)$$

Denaturation time as predictor of thermal lesion depth

Figure 7 shows the relationship between the denaturation time (TD) and the time required to achieve lesion depths of 2, 3 and 4 mm (t_{2mm}, t_{3mm} and t_{4mm}). In all cases TD was seen to be a good predictor ($R^2 > 0.96$, $p < 0.05$). The following mathematical relationships were found for each lesion depth:

$$t_{2mm} = 0.64 \times TD + 2.76 \quad (5)$$

$$t_{3mm} = 1.33 \times TD + 3.93 \quad (6)$$

$$t_{4mm} = 2.85 \times TD + 4.41 \quad (7)$$

DISCUSSION

Our goal was to find the mathematical expression relating the lesion depth created during RF cardiac ablation with the denaturation time measured from PS-OCR. The first step was to assess whether computer modeling could provide consistent results in physical terms. In this respect, Fig. 4 confirms that the 70ºC isotherm correlated well with the $\Omega = 4.6$ isoline, which corresponds to a 99% probability of cell death [38], while the 50ºC isotherm represents the thermal lesion reasonably well [17], which is obviously deeper than the fiber denaturation zone. The result shown in Figure 4(b) also seems reasonable, since a

previous experiment had shown that within the spatial window of PS-OCR (~0.75 mm), optical birefringence was completely lost within a short interval [15].

The computer results obtained also suggest a strong relationship between the evolution of lesion depth (related with the 50ºC isotherm) and TD. The first relationship analyzed (Eq. (4)) suggests that lesion depth can be estimated from a known TD value. For instance, if PS-OCR images indicate the complete loss of optical birefringence across the 0.75 mm spatial window at 12 s, it would be possible to estimate a lesion depth of 2.75 mm with 83% of variance in the fit. Interestingly, Eq. (4) also indicates that if denaturation is detected very early (i.e. TD almost zero), a lesion depth of 2.33 mm could have already been created. This can also be concluded from Equation (5): it is not possible to predict a lesion depth smaller than 2 mm by measuring denaturation time, as this depth has already been reached at that time. In contrast, Equations (6) and (7) could be used to predict the ablation time required to ensure a specific lesion depth. Eq. (6) suggests that a lesion depth of 3 mm will almost certainly be created if ablation time is prolonged accordingly. For instance, if denaturation time is detected at 10 s, an extension of ~7 s (i.e. a total time of $1.33 \times 10 + 3.93 = 17.23$ s) would ensure a minimum lesion depth of 3 mm. The same process can be followed with Eq. (7) to ensure a lesion depth of 4 mm.

Clinical importance

The present findings have important clinical implications in the context of real time monitoring of the progress of lesion depth during RF ablation of atrial fibrillation. As atrial wall thickness is ~2 mm [2], a depth around this value would be enough to produce

transmural lesions. If the lesion is not entirely transmural the treatment has failed, while if the lesion is too deep the esophagus could be thermally injured [39]. Our results suggest that using PS-OCR to measure denaturation time would provide the exact ablation time required to reach a specific, and hence transmural, lesion depth and thus minimize the risk of esophageal injury. These findings now need to be confirmed in actual clinical and pre-clinical scenarios.

Limitations

This study has certain limitations that need to be pointed out. Firstly, although RF cardiac ablation is always conducted using irrigated electrodes, we initially opted to model a non-irrigated electrode, since it provides simpler temperature distributions in which the hottest point is always close to the electrode-tissue interface. This means that all the tissue occupying the PS-OCR spatial window (0.75 mm under the tissue surface) is exposed to heating, as opposed to irrigated electrodes, where the hottest point is several millimeters away [40], so that the surface tissue may not be heated. Future studies should be conducted to confirm the utility of PS-OCR with irrigated electrodes.

Secondly, the esophagus and other adjacent structures were not included in the model, since this was an exploratory study and we were not interested in how PS-OCR technology works in the presence of a realistic pattern of surrounding tissues. However, in a previous computational study, we observed that the temperature distributions were hardly affected by the presence of the esophagus and other adjacent structures (lung, aorta, connective tissue, etc.) [41], since these organs and tissues have similar electrical and thermal

characteristics. We observed that the most important factor in damage to the esophagus was really the distance between the ablating electrode and the esophagus.

Thirdly, the model assumed healthy tissue properties. However, in a recent study, we assessed the thermal impact of the heterogeneity of pathological tissue (including fibrotic tissue and fat) during RF cardiac ablation [42] and observed that it did not have a significant impact on the thermal lesion size, since the density of the electrical current was only affected on a small-scale. However, the effect of including the specific optical properties of pathological tissue could be important in terms of birefringence loss and future experimental studies on the substrate of arrhythmia should take this issue into account. Unfortunately, to our knowledge, there is no experimental data available on the optical properties of the different arrhythmogenic substrates.

Future work should include the study of the variation of optical properties with temperature to compare the effects of laser ablation vs RF ablation.

CONCLUSIONS

The computer results confirmed the strong relationship between denaturation time (TD) and lesion depth. The mathematical relationships between TD (estimated by PS-OCR) and lesion depth could be used to provide the exact ablation time required to ensure a specific lesion depth.

ACKNOWLEDGEMENTS

This work was partially supported by the Spanish Government under the "*Plan Estatal de Investigación, Desarrollo e Innovación Orientada a los Retos de la Sociedad*" Grant "TEC2014-52383-C3 (TEC2014-52383-C3-1-R)". A. González-Suárez has a Postdoctoral Grant "Juan de la Cierva-formación" (FJCI-2015-27202) supported by the Spanish Ministerio de Economía, Industria y Competitividad. This study was partially presented at the 2017 Annual Meeting of the American Society for Laser Medicine and Surgery. A. González-Suárez received a travel grant from the United States Air Force Office of Scientific Research.

References

1. Maurer T, Kuck KH. The quest for durable lesions in catheter ablation of atrial fibrillation - technological advances in radiofrequency catheters and balloon devices. Expert Rev Med Devices 2017; doi: 10.1080/17434440.2017.1358086. [Epub ahead of print]
2. Sánchez-Quintana D, López-Mínguez JR, Macías Y, Cabrera JA, Saremi F. Left atrial anatomy relevant to catheter ablation. Cardiol Res Pract. 2014;2014:289720.
3. Marar D, Muthusamy V, Krishnan SC. Avoiding oesophageal injury during cardiac ablation: insights gained from mediastinal anatomy. Europace. 2017. doi: 10.1093/europace/eux024. [Epub ahead of print]
4. Kaneshiro T, Matsumoto Y, Nodera M, Kamioka M, Kamiyama Y, Yoshihisa A, Ohkawara H, Suzuki H, Takeishi Y. Anatomical predisposing factors of transmural thermal injury after pulmonary vein isolation. Europace. 2017. doi: 10.1093/europace/eux185. [Epub ahead of print]
5. Petersen HH, Chen X, Pietersen A, Svendsen JH, Haunsø S. Lesion Dimensions During Temperature-Controlled Radiofrequency Catheter Ablation of Left Ventricular Porcine Myocardium Impact of Ablation Site, Electrode Size, and Convective Cooling. Circulation. 1999;99(2):319-25.

6. Nakagawa H, Kautzner J, Natale A, Peichl P, Cihak R, Wichterle D, Ikeda A, Santangeli P, Di Biase L, Jackman WM. Locations of High Contact Force during Left Atrial Mapping in Atrial Fibrillation Patients: Electrogram Amplitude and Impedance Are Poor Predictors of Electrode-Tissue Contact Force for Ablation of Atrial Fibrillation. Circ Arrhythm Electrophysiol 2013; 6(4):746-53.
7. Reddy VY, Shah D, Kautzner J, Schmidt B, Saoudi N, Herrera C, Jaïs P, Hindricks G, Peichl P, Yulzari A, Lambert H, Neuzil P, Natale A, Kuck KH. The relationship between contact force and clinical outcome during radiofrequency catheter ablation of atrial fibrillation in the TOCCATA study. Heart Rhythm 2012;9(11):1789-95.
8. Pang GA, Bay E, Deán-Ben XL, Razansky D. Three-Dimensional Optoacoustic Monitoring of Lesion Formation in Real Time During Radiofrequency Catheter Ablation. J Cardiovasc Electrophysiol 2015;26(3):339-45.
9. Wang H, Kang W, Carrigan T, Bishop A, Rosenthal N, Arruda M, Rollins AM. In vivo intracardiac optical coherence tomography imaging through percutaneous access: toward image-guided radio-frequency ablation. J Biomed Opt. 2011;16(11):110505.
10. Ahmad I, Gribble A, Ikram M, Pop M, Vitkin A. Polarimetric assessment of healthy and radiofrequency ablated porcine myocardial tissue. J Biophotonics 2016;9(7):750-9.
11. Hitzenberger C, Goetzinger E, Sticker M, Pircher M, Fercher A. Measurement and imaging of birefringence and optic axis orientation by phase resolved polarization sensitive optical coherence tomography. Opt Express. 2001;9(13):780-790.
12. Haskell RC, Carlson FD, Blank PS. Form birefringence of muscle. Biophys J. 1989;56:401–413.
13. Yang X, Chin L, Klyen BR, Shavlakadze T, McLaughlin RA, Grounds MD, Sampson DD. Quantitative assessment of muscle damage in the mdx mouse model of Duchenne muscular dystrophy using polarization-sensitive optical coherence tomography. J Appl Physiol. 2013;115(9):1393-1401.
14. Park B, Saxer C, Srinivas SM, Nelson J, de Boer JF. In vivo burn depth determination by high-speed fiber-based polarization sensitive optical coherence tomography. J Biomed Opt 2001;6(4):474-79.

15. Herranz D, Lloret J, Jiménez-Valero S, Rubio-Guivernau JL, Margallo-Balbás E. Novel catheter enabling simultaneous radiofrequency ablation and optical coherence reflectometry. Biomed Opt Express 2015; 6(9):3268-75.
16. Herranz D, Jiménez-Valero S, Largo Aramburu C, Lloret J, Rubio-Guivernau JL, Margallo-Balbás E. Percutaneous RF ablation guided by polarization-sensitive optical coherence reflectometry in an integrated catheter: experimental evaluation of the procedure. J Innovations in Cardiac Rhythm Management 2015;6:2086–91.
17. Haines DE. Letter by Haines regarding article, "Direct measurement of the lethal isotherm for radiofrequency ablation of myocardial tissue". Circ Arrhythm Electrophysiol 2011;4(5):e67; author reply e68.
18. González-Suárez A, Gutierrez-Herrera E, Berjano E, Jimenez Lozano JN, Franco W. Thermal and elastic response of subcutaneous tissue with different fibrous septa architectures to RF heating: numerical study. Lasers Surg Med 2015;47(2):183-95.
19. Jimenez Lozano JN, Vacas-Jacques P, Anderson RR, Franco W. Effect of fibrous septa in radiofrequency heating of cutaneous and subcutaneous tissues: computational study. Lasers Surg Med 2013;45(5):326-38.
20. Ganguly M, Miller S, Mitra K. Model development and experimental validation for analyzing initial transients of irradiation of tissues during thermal therapy using short pulse lasers. Lasers Surg Med. 2015;47(9):711-22.
21. Li D, Li R, Jia H, Chen B, Wu W, Ying Z. Experimental and numerical investigation on the transient vascular thermal response to multi-pulse Nd:YAG laser. Lasers Surg Med 2017. doi: 10.1002/lsm.22695. [Epub ahead of print]
22. Cao H, Speidel MA, Tsai JZ, Van Lysel MS, Vorperian VR, Webster JG. FEM analysis of predicting electrode-myocardium contact from RF cardiac catheter ablation system impedance. IEEE Trans Biomed Eng 2002;49(6):520-6.
23. González-Suarez A, Berjano E. Comparative analysis of different methods of modeling the thermal effect of circulating blood flow during RF cardiac ablation. IEEE Trans Biomed Eng 2016;63(2):250-9.

24. Abraham JP, Sparrow EM. A thermal-ablation bioheat model including liquid-to-vapor phase change, pressure- and necrosis-dependent perfusion, and moisture-dependent properties. Int J Heat Mass Tran 2007;50(13-14):2537-44.
25. Byeongman J, Alptekin A. Prediction of the extent of thermal damage in the cornea during conductive keratoplasty. J Therm Biol 2010;35(4):167-74.
26. Pérez JJ, González-Suárez A, Berjano E. Numerical analysis of thermal impact of intramyocardial capillary blood flow during radiofrequency cardiac ablation. Int J Hyperth 2017;18:1-7.doi: 10.1080/02656736.2017.1336258. [Epub ahead of print]
27. Labonté S. Numerical model for radio-frequency ablation of the endocardium and its experimental validation. IEEE Trans Biomed Eng 1994; 41(2):108-15.
28. Doss JD. Calculation of electric fields in conductive media. Med Phys 1982; 9(4):566-73.
29. Pearce JA. Improving Accuracy in Arrhenius Models of Cell Death: Adding a Temperature-Dependent Time Delay. J Biomech Eng 2015;137(12):121006.
30. Pearce J. Mathematical models of laser-induced tissue thermal damage. Int J Hyperthermia 2011;27(8):741-50.
31. Hasgall PA, Di Gennaro F, Baumgartner C, Neufeld E, Gosselin MC, Payne D, Klingenböck A, Kuster N, "IT'IS Database for thermal and electromagnetic parameters of biological tissues," Version 3.0, September 01st, 2015, DOI: 10.13099/VIP21000-03-0. www.itis.ethz.ch/database.
32. Gopalakrishnan J. A mathematical model for irrigated epicardial radiofrequency ablation. Ann Biomed Eng 2002;30(7):884–93.
33. Schutt D, Berjano EJ, Haemmerich D. Effect of electrode thermal conductivity in cardiac radiofrequency catheter ablation : A computational modeling study. Int J Hyperth 2009; 25(2):99-107.
34. Haemmerich D, Chachati L, Wright AS, Mahvi DM, Lee FT, Webster JG. Hepatic radiofrequency ablation with internally cooled probes: effect of coolant temperature on lesion size. IEEE Trans Biomed Eng 2003; 50(4):493-9.
35. Berjano EJ. Theoretical modeling for radiofrequency ablation: state-of-the-art and challenges for the future. Biomed Eng Online 2006;5:24.

36. Tungjitkusolmun S, Vorperian VR, Bhavaraju N, Cao H, Tsai JZ, Webster JG. Guidelines for predicting lesion size at common endocardial locations during radio-frequency ablation. IEEE Trans Biomed Eng 2001;48(2):194-201.
37. Haemmerich D, Webster JG. Automatic control of finite element models for temperature-controlled radiofrequency ablation. Biomed Eng Online 2005;4:42.
38. Chang IA, Nguyen UD. Thermal modeling of lesion growth with radiofrequency ablation devices. Biomed Eng Online 2004;3(1):27.
39. Nair GM, Nery PB, Redpath CJ, Lam BK, Birnie DH. Atrioesophageal fistula in the era of atrial fibrillation ablation: a review. Can J Cardiol. 2014;30(4):388-95.
40. Demazumder D, Mirotznik MS, Schwartzman D. Biophysics of radiofrequency ablation using an irrigated electrode. J Interv Card Electrophysiol 2001;5(4):377-89.
41. Berjano EJ, Hornero F. What affects esophageal injury during radiofrequency ablation of the left atrium? An engineering study based on finite-element analysis. Physiol Meas 2005;26(5):837-48.
42. Pérez JJ, D'Avila A, Aryana A, Trujillo M, Berjano E. Can Fat Deposition After Myocardial Infarction Alter the Performance of RF Catheter Ablation of Scar-Related Ventricular Tachycardia?: Results from a Computer Modeling Study. J Cardiovasc Electrophysiol 2016;27(8):947-52.

Table 1. Thermal and electrical characteristics of the model elements [23].

Element/Material		**σ (S/m)**	**k (W/m·K)**	**ρ (kg/m^3)**	**c (J/kg·K)**
Electrode/Pt-Ir		4.6×10^{6}	71	21500	132
Thermistor/Glass fiber		10^{-5}	0.038	32	835
Catheter/Polyurethane		10^{-5}	0.026	70	1045
Cardiac chamber/Blood		0.667	0.54	1000	4180
Myocardium/ Cardiac tissue	Liquid phase	σ_o*	k_o*	ρ_l*	c_l*
	Gas phase			370.44	2155.92

*σ: electric conductivity; k: thermal conductivity; ρ: density; c: specific heat. These terms were varied according to Table 2.

Table 2. Range of variation of the model parameters.

Parameter		**Control**	**Max**	**Min**	**Ref.**
Tissue electrical conductivity	σ_o (S/m)	0.381	0.61	0.281	[31,32]
Tissue thermal conductivity	k_o (W/m·K)	0.56	0.60	0.50	[31]
Tissue density	ρ_l (kg/m^3) (liquid phase)	1081	1143	1059	[31]
Tissue specific heat	c_l (J/kg·K) (liquid phase)	3686	3724	3614	[31]
Thermal convective coefficient at the tissue-blood interface	h_T (W/m^{2}K)	110	121	99	
Thermal convective coefficient at the electrode-blood interface	h_E (W/m^{2}K)	1234	1357	1111	
Target temperature	T_{target} (ºC)	70	80	60	

Tissue characteristics were considered to be at 37ºC.

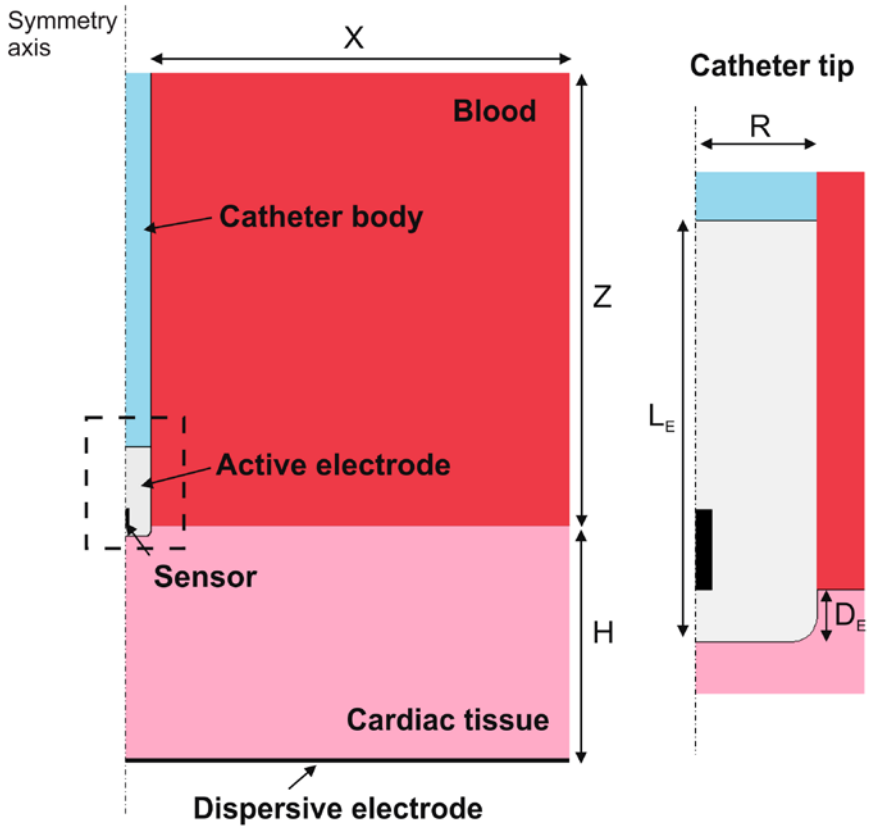

Figure 1 Geometry of the computational model and detail of the electrode tip. Dimensions X and Z (X=Z=40 mm) were checked to validate their sufficiency and avoid boundary problems. H: Thickness of cardiac tissue (20 mm), D_E: insertion depth of the electrode in the tissue (D_E=0.5 mm), L_E: electrode length (L_E=4 mm), R: catheter radius (R=1.165 mm). A temperature sensor (0.75 × 0.3 mm black rectangle) was assumed to be embedded in the electrode in order to simulate a constant temperature protocol.

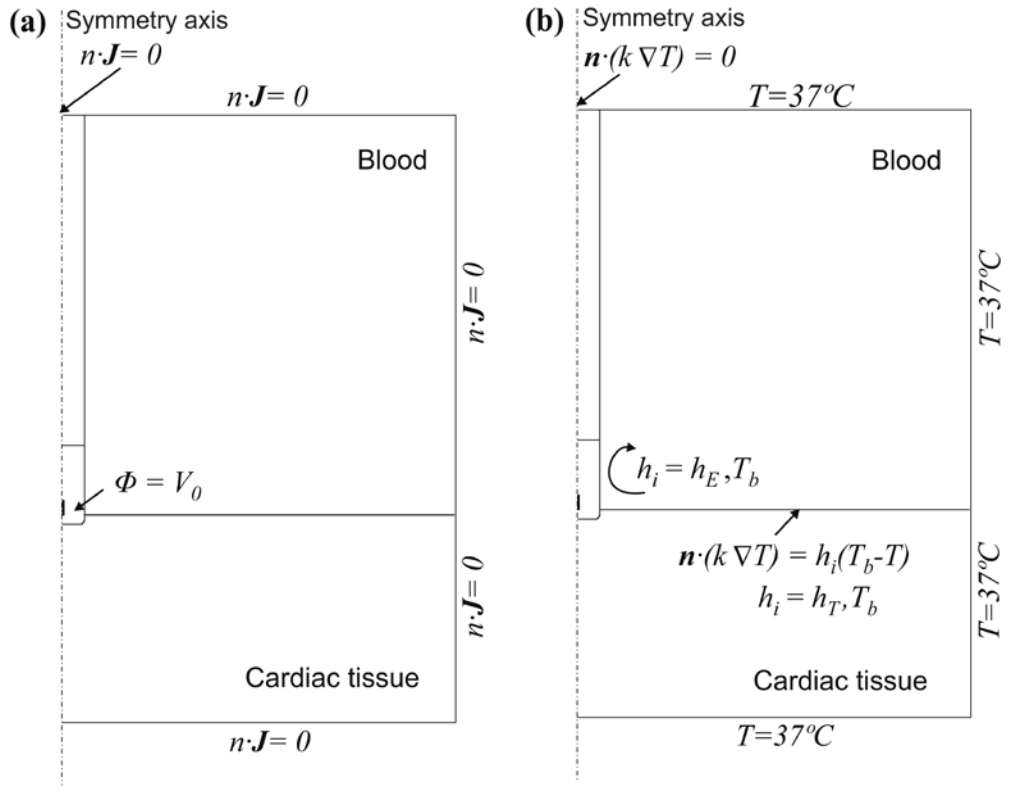

Figure 2 Electrical (a) and thermal (b) boundary conditions of the model. h_E and h_T are the thermal convection coefficients at the electrode–blood and the tissue–blood interfaces, respectively.

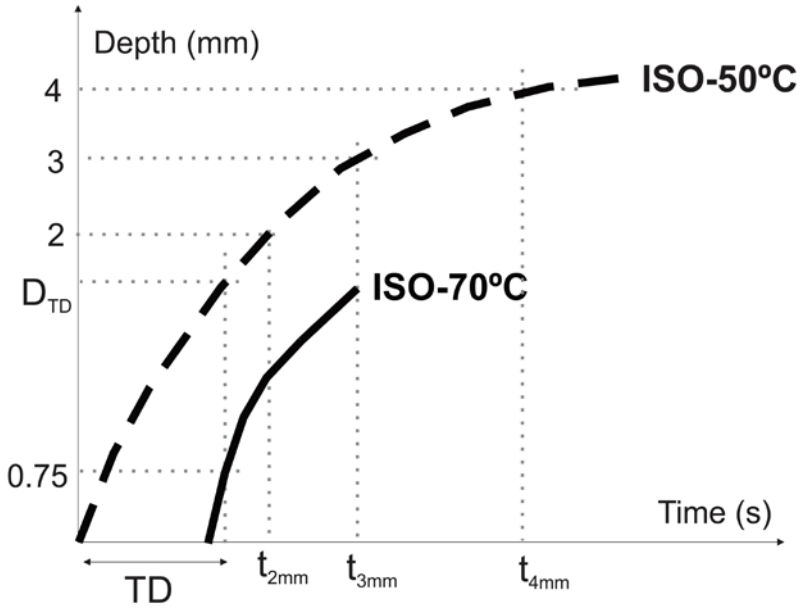

Figure 3 Our hypothesis was that there is a relationship between the progress of the thermal lesion depth assessed by the 50ºC isotherm (dashed line ISO-50ºC) and the change in fiber birefringence assessed by the 70ºC isotherm, (solid line ISO-70ºC). The objective was to obtain mathematical relationships between the denaturation time (TD, the time when the birefringence change measured by PS-ORC is detected at a depth of 0.75 mm) and the time required for the thermal lesion to reach a specific depth of 2, 3 or 4 mm (t_{2mm}, t_{3mm} and t_{4mm}).

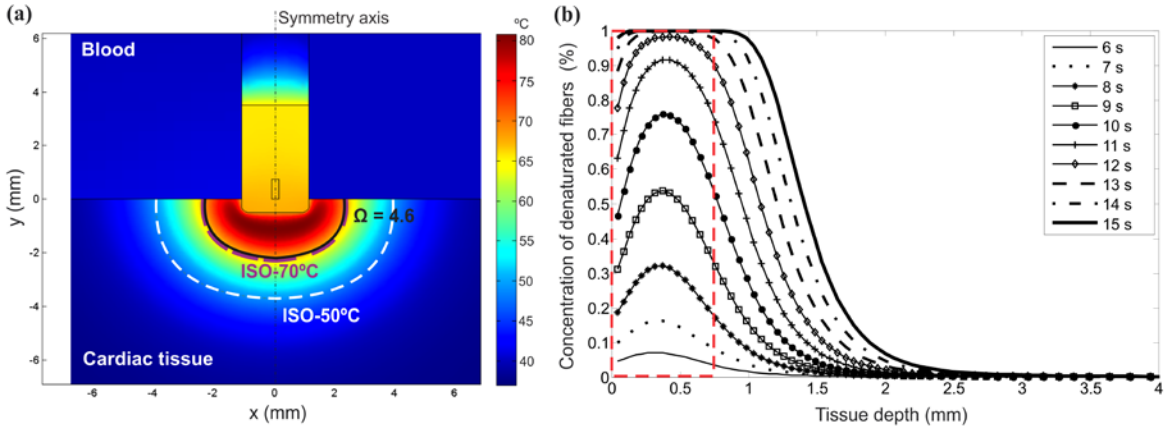

Figure 4 **(a)** Spatial temperature distribution around the ablation electrode at 15 s obtained from the computer model. The purple dashed line represents the 70ºC isotherm marking loss of birefringence by fiber denaturation. The white dashed line represents the 50ºC isotherm marking the onset of irreversible thermal damage. The black line is the contour of the zone representing a 99% probability of cell death (Ω=4.6). **(b)** Time course of the percentage of denatured fibers in the tissue across the symmetry axis *y*. The dashed box shows the spatial window detected by PS-OCR (0–0.75 mm). Note that complete fiber denaturation occurs at around 12 s of RF ablation.

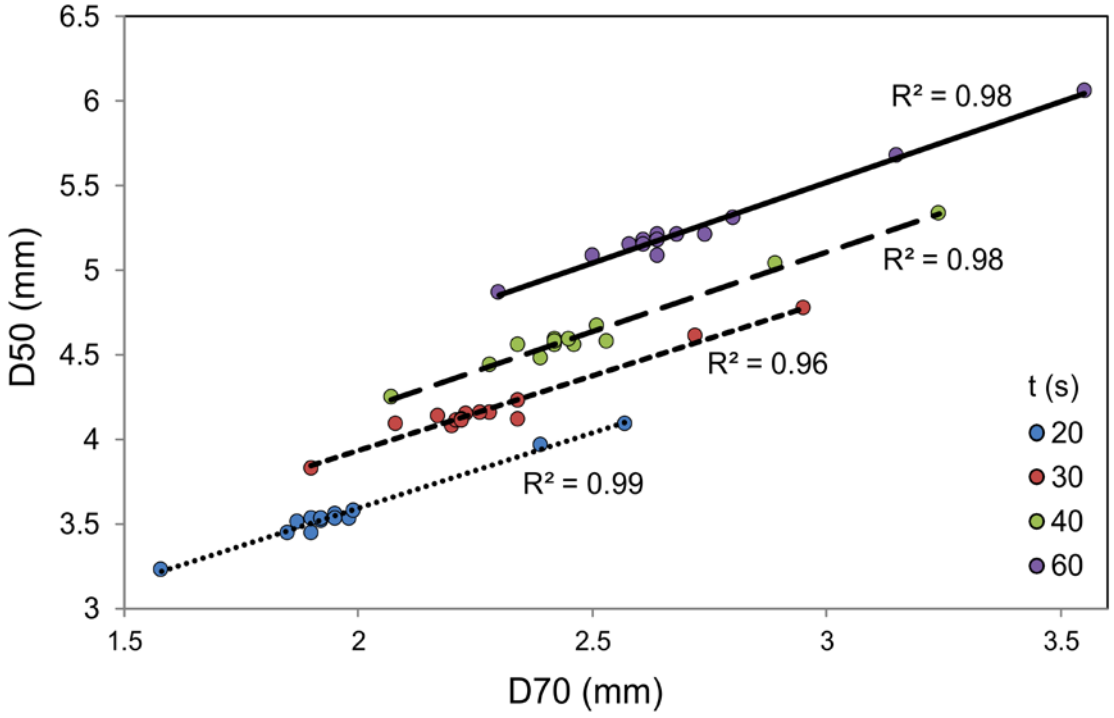

Figure 5 Relationship between the depths of the 50ºC and 70ºC isotherms (D50 and D70, respectively) at different times (from 20 to 60 s).

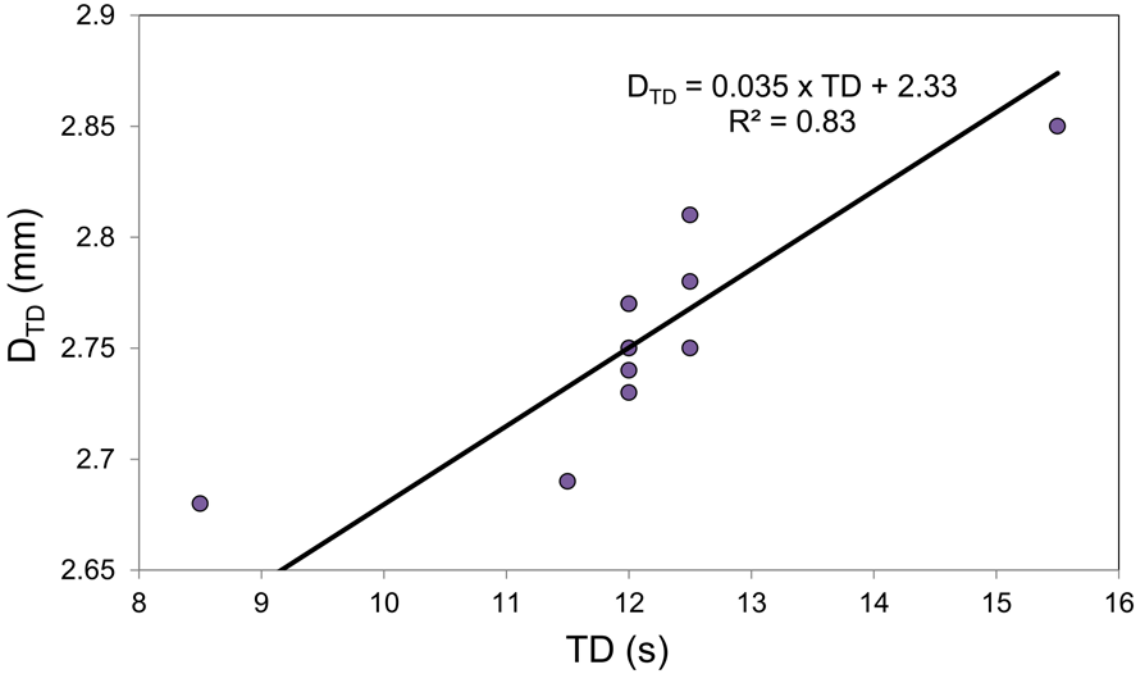

Figure 6 Relationship between the time at which the 70ºC isotherm reaches a depth of 0.75 mm (TD, denaturation time) and thermal lesion depth at that time (D_{TD}).

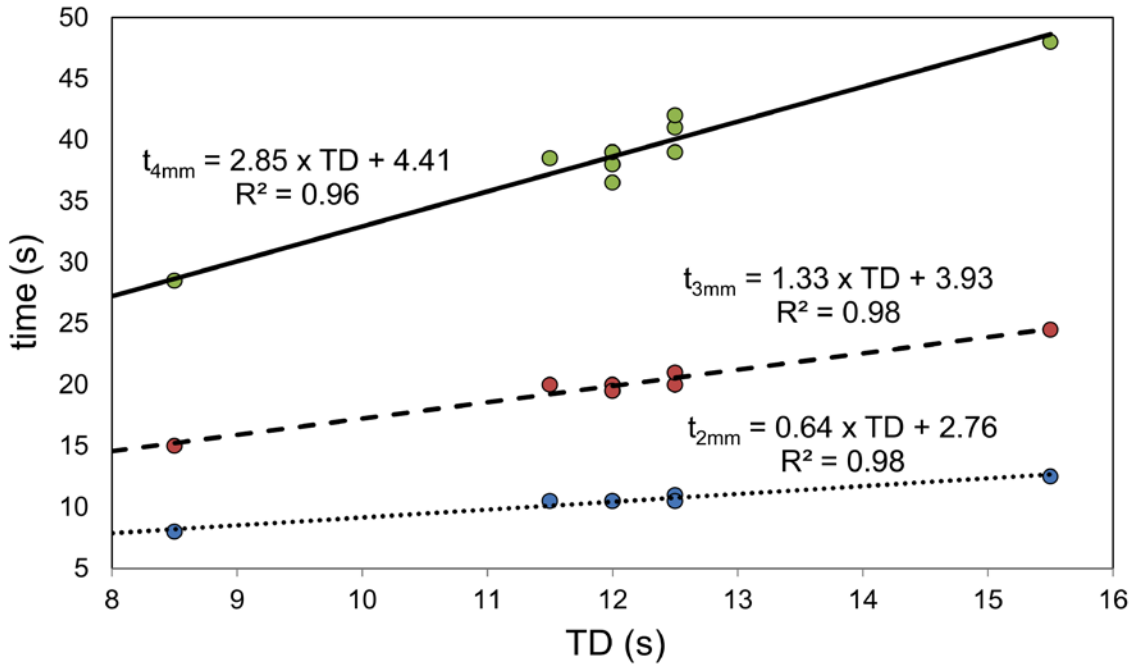

Figure 7 Relationship between the time when ISO-70ºC reaches a depth of 0.75 mm (TD) and the time required to achieve a lesion depth of 2 mm, 3 mm and 4 mm (t_{2mm}, t_{3mm} and t_{4mm}).